An Amyloid Organelle: Solid State NMR Evidence for Cross-Beta Assembly of Gas Vesicles *

Marvin J. Bayro,[‡,‖] Eugenio Daviso,[‖,¶] Marina Belenky,[¶] Robert G. Griffin,[‡,‖] Judith Herzfeld[¶,1]

From the [‡]Department of Chemistry, Massachusetts Institute of Technology, Cambridge, MA 02139, [‖]Francis Bitter Magnet Laboratory, Massachusetts Institute of Technology, Cambridge, MA 02139, and [¶]Department of Chemistry, Brandeis University, Waltham, MA 02454

*Running Title: *An Amyloid Organelle*

[1]To whom correspondence should be addressed: Judith Herzfeld, Department of Chemistry, Brandeis University, Waltham, MA 02454-9110, USA, Tel.: (781) 736-2538; Fax: (781) 736-2516; E-mail herzfeld@brandeis.edu

Keywords: Amyloid, Cyanobacteria, Protein Self-Assembly, Protein-Protein Interactions, Solid-State NMR Spectroscopy, Magic-Angle Spinning, Air-Water Interface

Background: The gas vesicles of aquatic microorganisms are hollow proteinaceous shells with remarkable physical properties that enable them to function as floatation organelles.
Result: The gas vesicle subunits associate in a cross-beta arrangement.
Conclusion: The gas vesicle wall constitutes a functional amyloid.
Significance: This new category of functional amyloid broadens our understanding of the diverse roles of the amyloid fold.

SUMMARY

Functional amyloids have been identified in a wide range of organisms, taking on a variety of biological roles, and being controlled by remarkable mechanisms of directed assembly. Here we report that amyloid fibrils constitute the ribs of the buoyancy organelles of *Anabaena flos-aquae*. The walls of these gas-filled vesicles are known to comprise a single protein, GvpA, arranged in a low-pitch helix. However, the tertiary and quaternary structures have been elusive. Using solid-state NMR correlation spectroscopy we find detailed evidence for an extended cross-β structure. This amyloid assembly helps to account for the strength and amphiphilic properties of the vesicle wall. Buoyancy organelles thus dramatically extend the scope of known functional amyloids.

Introduction

Found in a wide variety of organisms and associated with pathological and functional states, amyloids are open-ended protein assemblies characterized by a highly ordered cross-β architecture in which the β-strands are oriented transverse to the polymerization axis (1-3). Amyloid fibrils have been observed in a large number of pathologies, including neurodegenerative disorders and systemic amyloidoses (1). However, the discovery of *in vitro* fibril formation by proteins unrelated to disease has led to the notion that amyloid is a generic and accessible state in the protein folding landscape (4). Moreover, proteins in organisms ranging from bacteria to mammals have been found to form amyloid structures that carry out specific functions and are referred to as functional amyloids (5). While functional amyloids share the general morphology of disease-related amyloids, they possess key distinctive features related to the control of fibril formation. These include sequestration of the proteins to avoid aberrant fibril formation, rapid fibril elongation that avoids the accumulation of intermediates, and regulation of both assembly and disassembly (6). Thus the discovery and study of functional amyloid systems have provided new insights into the diverse ways in which proteins adopt amyloid structures (7).

Gas vesicles are buoyancy organelles that enable aquatic microorganisms to regulate their depth in the water column for optimal access to light and nutrients (8). The gas vesicle wall consists almost exclusively of a single protein, gas vesicle protein A (GvpA)[2], one of the most hydrophobic proteins known, while other proteins in the gas vesicle gene cluster either provide additional strength by binding to the exterior surface of the vesicle wall or appear to have roles in the assembly process (8). Figure 1 shows a schematic of the overall organization of gas vesicles. Early electron microscopy revealed ribbed spindles {Jost, 1970 #66} which, at higher resolution proved to be bipolar with low pitch helices forming the ribs {Offner, 1998 #14}. X-ray diffraction studies determined the thickness of the vesicle wall and the dimensions of the unit cell within the wall {Blaurock, 1976 #52}. These were found to be consistent with the size of the GvpA monomer. In addition, the x-ray diffraction showed reflections characteristic of β-sheets with strands oriented at an angle of 36° relative to the long axis of the vesicle. These last features have recently been confirmed by atomic force microscopy {McMaster, 1996 #13}.

Figure 1 also shows a recently proposed model of the quaternary structure involving an asymmetric dimer repeat unit (12). The model was initially developed based on the secondary structure propensity of the sequence, the positions of conserved residues among different organisms, electrostatic energy considerations, and the x-ray determined tilt of the β-strands relative to the vesicle axis (12). In this model, GvpA monomers contain a β-hairpin that forms an antiparallel β-sheet within the monomer. This β-sheet is extended by anti-parallel association of the β-sheets in adjacent monomers. A key to fulfilling the above considerations is that the center of the β-turn alternates between V34 and G35 in neighboring monomers.

Previous solid-state nuclear magnetic resonance (NMR) studies have provided support for the secondary structures inherent in the model: the asymmetric dimer repeat unit is consistent with duplicated resonances found in the initial study (12) and further experiments revealed that the protein backbone adopts a coil-alpha-beta-beta-alpha-coil conformation, in close agreement with the secondary structure tendency of the protein sequence (13). Here we show that the β-strands of GvpA form form the contacts predicted by the model. It thus appears that the gas vesicle wall comprises a helically wound amyloid fibril.

EXPERIMENTAL PROCEDURES

Preparation of gas vesicles – Cells of *Anabaena flos-aquae* (strain 1403/13f, Cambridge Collection of Algae and Protozoa, Cambridge, UK) were grown in an atmosphere containing $^{13}CO_2$ and $^{15}N_2$ to produce uniformly ^{13}C and ^{15}N labeled cells. Floating cells were collected and lysed to release gas vesicles which were isolated and washed by repeated floatation as described previously (12). Washed vesicles were collapsed by a pressure pulse, pelleted by centrifugation, and packed into 3.2 mm rotors, with approximately 24 mg of sample per rotor.

Solid-state NMR spectroscopy – MAS NMR experiments were performed using a custom-designed spectrometer (D. J. Ruben, Francis Bitter Magnet Laboratory, Cambridge, MA) operating at 700 MHz ^1H Larmor frequency and equipped with a triple-resonance $^1H/^{13}C/^{15}N$ Varian-Chemagnetics (Palo Alto, CA) probe fitted with a 3.2 mm MAS stator. Preliminary correlation spectra were recorded using various schemes for ^{13}C-^{13}C recoupling, including proton-assisted recoupling (PAR) (14), proton-driven spin diffusion (15), dipolar assisted rotational resonance (DARR) (16,17), and band-selective radio frequency-driven recoupling (18). PAR and DARR spectra, recorded with 10 ms and 250 ms mixing periods, respectively, presented optimal sensitivity in these uniformly ^{13}C-labeled samples and were selected for further analysis. Two-dimensional spectra were acquired with 256 indirect points, with a 60 ms dwell time and 320 transients per point. High-power, two-pulse phase modulation ^1H decoupling (19) was applied during the evolution and detection periods.

Structural modeling – Representations of GvpA assembly based on the asymmetric dimer model were generated using CNS version 1.2 by

applying the simulated annealing protocol (20). The structure was constrained by the backbone torsion angles obtained from chemical shift analysis, hydrogen bonds between putative β-strands, and translational symmetry between dimers. Calculations were performed in three stages, using an NOE potential. High temperature annealing was carried out by performing molecular dynamics at 50000 K for 15 ps in torsion space starting from randomized coordinates. The NOE and dihedral angle restraints were applied with force constants of 150 kcal $Å^{-2}$ and 100 kcal $Å^{-2}$ respectively. This was followed by fast cooling from 50000 K to 3000 K, in steps of 250 K, with an evolution time of 15 ps at each temperature. The final slow cooling, from 3000 K to 0 K, was carried out in steps of 25 K with an evolution time of 15 ps at each temperature. Typically, a set of 60 structures was generated for each calculation, and the average of these structures was calculated and minimized. The results were visualized with VMD (21).

RESULTS

As shown in Figure 1, the proposed model presents four different interfaces between strands, two intramolecular and two intermolecular. The intramolecular interfaces are between the N- and C-terminal portions of the β-hairpin within each of the two types of monomers. The intermolecular interfaces are between the N(C)-terminal segment of the hairpin of one monomer and the N(C)-terminal segment of the hairpin of the adjacent monomer. Having previously assigned 80% of the GvpA resonances in uniformly ^{13}C and ^{15}N labeled gas vesicles of *Anabaena flos-aquae* (13), we sought to validate our model by checking for the predicted interactions between β-strands in long-range correlation spectra. For this purpose, multiple sets of ^{13}C-^{13}C dipolar correlation spectra were recorded under different experimental conditions. The hypothetical model guided our analysis by focusing on potential interstrand contacts within 6 Å, the approximate limit of the dipolar interactions probed by our experiments. Of particular significance are contacts between β-strand residues that are far apart in the primary sequence because they provide strong evidence for interstrand interfaces. For example, as shown in Figure 1, the model has I23 opposite I47 across the intramolecular interfaces of G-turn monomers and opposite I45 across the intramolecular interfaces of V-turn monomers. Similarly, the model has L39 opposite I47 across the intermolecular interface between C-terminal segments and I23 opposite L33 across the intermolecular interface between N-terminal segments.

As shown in Figure 2, contacts corresponding to interactions between the above residue pairs are observed as cross-peaks in the ^{13}C-^{13}C correlation spectra. Numerous other predicted correlations are also observed, as summarized in Table 1 and Figure 3. In particular, backbone–side-chain and side-chain–side-chain contacts are observed between many pairs of residues opposing one another in the proposed β-strand interfaces.

These solid-state NMR correlations represent the first residue-level characterization of the supramolecular architecture of the gas vesicle wall. Taken together, they assert topological constraints that are probably impossible to satisfy in self-consistent fashion outside the extended, antiparallel β-sheet arrangement of our model. Some observed correlations are difficult to explain without turns in adjacent monomers that are shifted by one residue. For example, I45 shows correlations with both I25 and I23, while I23 shows correlations with both I47 and I45. Other observed correlations, require interstrand contacts. For example, the extended secondary structure precludes intrastrand contacts between D26 and R30 and between L39 and I47. Taken together, the correlations strongly support the proposed model.

DISCUSSION

Core β-sheet structure of gas vesicles

The structural constraints described above indicate that the intermolecular association between GvpA subunits along the winding filament that forms the ribs of the gas vesicle wall is primarily mediated by β-sheet formation on both sides of the β-hairpin. Thus the β-strands in the middle of the amino acid sequence form the core of the GvpA assembly in the direction of the

rib, approximately perpendicular to the long vesicle axis. This is at variance with a recently reported model involving docking of prefolded monomers (23). However, that work made use of a single monomer fold, rather than two folds differing in the location of the β-turn. Furthermore, that fold was optimized in bulk solvent, rather than at an air-water interface, and it was not allowed to adapt to interactions with neighbors during docking. The result was a two-dimensional array with holes within and between ribs that make it resemble a sieve more than a barrier. It is difficult to reconcile such a structure with the physical properties of the gas vesicle wall.

The question remains what roles are played by the GvpA sequences that flank the β-strands. In our model, these segments are attached to the edges of the amyloid ribbons at locations corresponding to the interfaces between the gas vesicle ribs (see Figure 4). Such an arrangement is consistent with the transverse ridges that are observed in electron micrographs and atomic-force micrographs of gas vesicles (10). Mass spectrometry shows that the helices and coils of gas vesicle are largely protected from proteolysis (24), and solid-state NMR spectra indicate that they are largely rigid (13). We therefore expect the helices and coils to be constrained by yet-to-be determined interactions with other parts of the assembly, allowing them to hold the ribs together.

The major physical characteristics of the gas vesicle wall, including its architecture, structural strength and interfacial stability, reflect the general features of the core β-sheet structure within the ribs. The inter-rib spacing is determined by the length of the β-strand segments and their inclination from the vesicle axis (see Figure 1). The strand orientation also sets the hydrogen bonds at an angle that provides equal strength along and transverse to the cylinder axis (8). In addition, the sequences in the β-strands are such that one surface of the β-sheet is highly hydrophobic and likely responsible for precluding water condensation inside the vesicles. Therefore, the cross-β core structure of the gas vesicle rib allows for formation of a resilient supramolecular assembly that can stabilize an air-water interface.

Some of the above structural features resemble morphological properties generally found in amyloid fibrils. The cross-β assembly along the rib of the gas vesicle wall is similar to the ribbon-like structure formed by amyloid fibrils, which often presents a twist that arises from the inherent left-handed twist of β-sheets formed by L-amino acids (25). Instead of a twist, the ribs of gas vesicles curl around the long vesicle axis to produce the cylindrical shape of the wall. While the twist of amyloid fibrils thus appears to be an incidental feature of generic extended β-sheet structures, the curl of gas vesicle ribs serves a specific purpose in the formation and elongation of this organelle. Furthermore, just as the pitch of the twist varies among amyloid fibrils, gas vesicles from different organisms are found with different diameters that depend on the sequence of the GvpA (8). Finally, amyloid fibrils often consist of multiple, laterally arranged protofilaments, held together by lateral interactions at the edges of the cross-β core. In the same way, amyloid in adjacent ribs of the gas vesicle wall must interact laterally to secure the overall assembly.

The gas vesicle ribs differ from other amyloid fibrils in two notable respects. First, the β-strands of gas vesicles cross the fibril at 54° to the fibril axis, rather than at a canonical ~90°. As noted elsewhere, this tilt contributes to the mechanical strength of the gas vesicles (8), a feature that is presumably irrelevant for pathological amyloids and relatively unimportant for the other functional amyloids. Second, the β–strands in gas vesicles are arranged anti-parallel fashion, rather than the more common parallel (usually, but not always, in-register) configuration {Shewmaker, 2011 #65}. This is another feature that is expected to contribute to the strength of the vesicle wall because the straight hydrogen bonds of anti-parallel β-sheets are stronger than the bent hydrogen bonds of parallel β-sheets.

Amyloid formation and the air-water interface

Hydrophobic-hydrophilic interfaces, have been found to enhance the self-assembly of a variety of amyloid-forming peptides into β-sheets,

both parallel and antiparallel. For example, Amyloid-β peptide, associated with Alzheimer's disease, has an amphipathic character and forms β-sheets at air-water interfaces (26). Similarly, recent studies have revealed the critical role of hydrophobic-water interfaces in driving fibril formation by islet amyloid polypeptide and α-Synuclein, peptides associated with type 2 diabetes and Parkinson's disease, respectively (27,28). In gas vesicles, it is to be expected that the air-water interface developed by the hydrophobic interior of the gas vesicle wall has the reciprocal effect of stabilizing the amyloid structure of the ribs and facilitating the incorporation of GvpA subunits during vesicle growth.

Current models of hydrophobin assembly (29,30) are based on compact subunits oriented by a hydrophobic patch into the air-water interface, where they join together to form intermolecular β-barrels. Whereas these secreted amphipathic proteins respond to air-exposed environments, the air-water interface in gas vesicles is itself developed by the gas vesicle wall. For this more rigorous purpose, the continuous hydrophobic surface of β-sheets that are co-planar with the air-water interface seems better suited than discrete hydrophobic patches on the surface of β-barrel units and resembles more closely the β-sheets formed by disease-related amyloidogenic peptides at hydrophobic-hydrophilic interfaces.

Function and secondary structure tendencies

The functional fold of GvpA in the gas vesicle wall contains structural elements consistent with the secondary structure propensity of the amino acid sequence. The high level of sequence conservation in these structural elements (12) is indicative of a highly evolved protein sequence selected for structural integrity in the context of a functional intermolecular assembly. This is in contrast to natively globular proteins that form amyloid fibrils under denaturing conditions. In such cases, the secondary structure of the amyloid state tends to deviate from the secondary structure propensity of the amino acid sequence and instead agrees more closely with the elements predicted by the aggregation properties of the sequence (31,32). On the other hand, several current models of the assembly of functional amyloids appear to be consistent with preservation of the secondary structure tendencies of the amino acid sequence. For example, supramolecular models of CsgA, the main constituent of curli fibers, are based on repeating segments with sequences predicted to adopt β-strand conformations (33). In the amyloid assembly of hydrophobins, which are soluble and some of which have known monomeric structures, the antiparallel β-sheets present in the monomeric fold are likely to be preserved after polymerization and flexible loops at each end of the cylindrical monomer appear to establish intermolecular interactions. One of these two loops, disordered in monomer form, is predicted to adopt a β-sheet conformation according to sequence analysis and evidently induces a β-sheet conformation in its partner (30). Therefore the correspondence between sequence tendency and secondary structure in the amyloid form found in GvpA may be a general feature of functional amyloids, reflecting the evolution of these systems to reach and maintain their assembled state.

Gas vesicles are only soluble in highly protic solvents and the monomers form amorphous precipitates when such solvents are dialyzed away. It is not fully understood how misfolding of GvpA is avoided in the cell, but since the expression of multiple gas vesicle genes is required for gas vesicle formation, other proteins in this gene cluster may transport GvpA and assist its insertion into the growing vesicle. Mechanisms to prevent aggregation have been recognized in other functional amyloids. The Ma component of Pmel17 self-assembles very rapidly, at rates that are several orders of magnitude faster than those of disease-related peptides (34). It has been suggested that these kinetics prevent the accumulation of intermediates that may lead to unwanted structures (5,34). Hydrophobin SC3 contains several highly conserved disulfide bridges that are responsible for its solubility when fully immersed in the aqueous environment, such that self-assembly only occurs when triggered by a hydrophobic interface (35). CsgA proteins require

the expression of additional genes for export, anchoring, and *in vivo* curli formation, but not for self-assembly once outside the cell. In this system, at least two other proteins function as chaperones to prevent unwanted aggregation of CsgA (6). The assembly of GvpA into gas vesicles seems to be controlled in a fashion similar to that of CsgA assembly into curli, with the further requirement of the *de novo* formation of an air-water interface.

REFERENCES

1. Chiti, F., and Dobson, C. M. (2006) *Annu. Rev. Biochem.* **75**, 333-366
2. Eanes, E. D., and Glenner, G. G. (1968) *J. Histochem. Cytochem.* **16**, 673-677
3. Sunde, M., Serpell, L. C., Bartlam, M., Fraser, P. E., Pepys, M. B., and Blake, C. C. F. (1997) *J. Mol. Biol.* **273**, 729-739
4. Dobson, C. M. (1999) *Trends Biochem. Sci.* **24**, 329-332
5. Fowler, D. M., Koulov, A. V., Balch, W. E., and Kelly, J. W. (2007) *Trends Biochem. Sci.* **32**, 217-224
6. Smith, A. M., and Scheibel, T. (2010) *Macromol. Chem. Physic.* **211**, 127-135
7. Otzen, D., and Nielsen, P. (2008) *Cell. Mol. Life Sci.* **65**, 910-927
8. Walsby, A. E. (1994) *Microbiol. Rev.* **58**, 94-144
9. Blaurock, A. E., and Walsby, A. E. (1976) *J. Mol. Biol.* **105**, 183-199
10. McMaster, T. J., Miles, M. J., and Walsby, A. E. (1996) *Biophys. J.* **70**, 2432-2436
11. Offner, S., Ziese, U., Wanner, G., Typke, D., and Pfeifer, F. (1998) *Microbiology* **144**, 1331-1342
12. Sivertsen, A. C., Bayro, M. J., Belenky, M., Griffin, R. G., and Herzfeld, J. (2009) *J. Mol. Biol.* **387**, 1032-1039
13. Sivertsen, A. C., Bayro, M. J., Belenky, M., Griffin, R. G., and Herzfeld, J. (2010) *Biophys. J.* **99**, 1932-1939
14. De Paëpe, G., Lewandowski, J. R., Loquet, A., Böckmann, A., and Griffin, R. G. (2008) *J. Chem. Phys.* **129**, 245101
15. Szeverenyi, N. M., Sullivan, M. J., and Maciel, G. E. (1982) *J. Magn. Reson.* **47**, 462-475
16. Takegoshi, K., Nakamura, S., and Terao, T. (2001) *Chem. Phys. Lett.* **344**, 631-637
17. Morcombe, C. R., Gaponenko, V., Byrd, R. A., and Zilm, K. W. (2004) *J. Am. Chem. Soc.* **126**, 7196-7197
18. Bayro, M. J., Maly, T., Birkett, N. R., Dobson, C. M., and Griffin, R. G. (2009) *Angew. Chem. Int. Ed.* **48**, 5708-5710
19. Bennett, A. E., Rienstra, C. M., Auger, M., Lakshmi, K. V., and Griffin, R. G. (1995) *J. Chem. Phys.* **103**, 6951-6958
20. Brunger, A. T., Adams, P. D., Clore, G. M., DeLano, W. L., Gros, P., Grosse-Kunstleve, R. W., Jiang, J.-S., Kuszewski, J., Nilges, M., Pannu, N. S., Read, R. J., Rice, L. M., Simonson, T., and Warren, G. L. (1998) *Acta Cryst. D* **54**, 905-921
21. Humphrey, W., Dalke, A., and Schulten, K. (1996) *J. Molec. Graphics* **14**, 33-38
22. Khurana, R., Uversky, V. N., Nielsen, L., and Fink, A. L. (2001) *J. Biol. Chem.* **276**, 22715-22721
23. Strunk, T., Hamacher, K., Hoffgaard, F., Engelhardt, H., Zillig, M. D., Faist, K., Wenzel, W., and Pfeifer, F. (2011) *Mol. Microbiol.* **81**, 56-68
24. Belenky, M., Meyers, R., and Herzfeld, J. (2004) *Biophys. J.* **86**, 499-505
25. Fändrich, M. (2007) *Cell. Mol. Life Sci.* **64**, 2066-2078
26. Schladitz, C., Vieira, E. P., Hermel, H., and Möhwald, H. (1999) *Biophys. J.* **77**, 3305-3310
27. Jean, L., Lee, C. F., Lee, C., Shaw, M., and Vaux, D. J. (2010) *FASEB J.* **24**, 309-317

28. Pronchik, J., He, X., Giurleo, J. T., and Talaga, D. S. (2010) *J. Am. Chem. Soc.* **132**, 9797-9803
29. Hakanpää, J., Paananen, A., Askolin, S., Nakari-Setälä, T., Parkkinen, T., Penttilä, M., Linder, M. B., and Rouvinen, J. (2004) *J. Biol. Chem.* **279**, 534-539
30. Kwan, A. H. Y., Winefield, R. D., Sunde, M., Matthews, J. M., Haverkamp, R. G., Templeton, M. D., and Mackay, J. P. (2006) *Proc. Natl. Acad. Sci. USA* **103**, 3621-3626
31. Tartaglia, G. G., Pawar, A. P., Campioni, S., Dobson, C. M., Chiti, F., and Vendruscolo, M. (2008) *J. Mol. Biol.* **380**, 425-436
32. Bayro, M. J., Maly, T., Birkett, N. R., MacPhee, C. E., Dobson, C. M., and Griffin, R. G. (2010) *Biochemistry* **49**, 7474-7484
33. Hammer, N. D., Schmidt, J. C., and Chapman, M. R. (2007) *Proc. Natl. Acad. Sci. USA* **104**, 12494-12499
34. Fowler, D. M., Koulov, A. V., Alory-Jost, C., Marks, M. S., Balch, W. E., and Kelly, J. W. (2006) *PLoS Biol.* **4**, e6
35. de Vocht, M. L., Reviakine, I., Wösten, H. A. B., Brisson, A., Wessels, J. G. H., and Robillard, G. T. (2000) *J. Biol. Chem.* **275**, 28428-28432

Acknowledgements – We thank Astrid Sivertsen, Kendra Frederick, Galia Debelouchina, and Vladimir Michaelis for insightful discussions, and Ajay Thakkar and David Ruben for technical assistance.

Footnotes

*This work was supported by NIH grants EB001035, EB003151, and EB002026.

[1]To whom correspondence should be addressed: Judith Herzfeld, Department of Chemistry, Brandeis University, Waltham, MA 02454-9110, USA, Tel.: (781) 736-2538; Fax: (781) 736-2516; E-mail herzfeld@brandeis.edu

[2]The abbreviations used are: GVpA, Gas vesicle protein A; MAS, magic-angle spinning; CsgA, curli subunit protein A; PAR, proton-assisted recoupling; DARR, dipolar-assisted rotational resonance.

FIGURE LEGENDS

FIGURE 1. Gas vesicle architecture and GvpA folding hypothesis. The gas vesicle is a ribbed cylinder with conical end caps. The ribs of the vesicle comprise GvpA monomers assembled in a low pitch helix. The horizontal lines shown within one of these ribs illustrate the orientation of the β-strands of GvpA as determined by x-ray diffraction.(8) The expanded view of this rib shows the asymmetric dimer model of the β-strands proposed by Sivertsen et al.(12) This model includes β-hairpins at G35 and V34 in alternating monomers, resulting in four different interfaces within the β-sheet. From top-to bottom, these are: G_C-G_N between the C- and N-terminal portions of the β-hairpin of a G-turn monomer; G_N-V_N between the N-terminal portions of the β-hairpins of the G-turn monomer and the adjacent V-turn monomer; V_N-V_C between the N- and C-terminal portions of the β-hairpin of the V-turn monomer; and V_C-G_C between the C-terminal portions of the β-hairpins of the V-turn monomer and the succeeding G-turn monomer.

FIGURE 2. Examples of NMR correlations between β-strand residues that are distant in the primary sequence. Details of the annealed asymmetric dimer model are shown on the left and examples of corresponding correlations are shown on the right. From top to bottom: The G_C–G_N interface represented by I47 and I23 in a single G-turn subunit; the G_N–V_N interface represented by I23 in a G-turn subunit and L33 in a V-turn subunit; the V_N–V_C interface represented by I23 and I45 in a single V-turn subunit; and

the V_C–G_C interface represented by L39 in a V-turn subunit and I47 in the neighboring G-turn subunit. The green, blue, and red colors on the left denote polar, basic, and acidic residues, respectively. Each spectrum on the right is a portion of either the 10 ms PAR spectrum (third from the top) or the 250 ms DARR spectrum (the other three). The full spectra are shown in the online Supporting Data.

FIGURE 3. Interstrand correlations between residues across the four different interfaces of the β-sheet assembly. The four interface labels are as defined in the legend to Figure 1. The numeral in the circle between two residues indicates the number of observed ^{13}C-^{13}C correlations assigned in each case (see Table 1).

FIGURE 4. Model of the amyloid ribbon segment formed by three GvpA molecules, illustrating possibilities for rib-rib interactions. The α-helical and coil portions of GvpA are included without any tertiary constraints. Located at the edges of the amyloid ribbon, they are well situated to be involved in rib-rib interactions that are likely to also include the turn portions of the β-strands.

TABLE 1. Correlations observed in ^{13}C-^{13}C spectra that correspond to inter-residue interactions along the four β-strand interfaces in our model of gas vesicle organization. These correlations are based on resolved cross-peaks assigned according to chemical shifts published previously (13), except for those in the segment V29-L33, which were identified subsequently. (*) Identifies correlations found in the DARR spectrum using a mixing time of 250 ms. (^) Identifies correlations found in the PAR experiment using a mixing time of 10 ms.

G_C-G_N	G_N-V_N	V_N-V_C	V_C-G_C
I47CG2-I23CB*^	I23CD1-L33CA*	S32CA-I36CD1*^	E37CB-S49CB*^
I47CD1-I23CB*^	I23CG2-L33CA*	S32CB-I36CB*	L38CB-A48CA*^
V46CB-V24CG1*^	V24CG1-S32CA*^	V31CG2-E37CB*^	L38CB-A48CB*^
I45CB-I25CG2*^	I25CG1-V31CG2*^	V29CG1-L39CG2*^	L38CG-A48CA*^
I45CD1-I25CG2*	I25CG2-V31CB*^	A27CB-I41CD1*^	L39CA-I47CA*
R44CB-D26CB*	D26CB-R30CG*^	D26CB-E42CA*	L39CA-I47CB*
E42CB-W28CB*	D26CB-R30CD*^	D26CB-E42CB*	L39CD1-I47CG2*^
I41CG1-V29CG1*^		I25CG2-A43CB*^	L39CD2-I47CB*^
I41CD1-V29CG1*^		V24CG1-R44CD*	L39CD2-I47CG2*^
I41CD1-V29CG2*		V24CG2-R44CD*	A40CA-V46CA*^
A40CB-R30CD*^		I23CG2-I45CA*	A40CB-V46CB*^
L38CG-S32CA*^		I23CD1-I45CA*^	I41CA-I45CD1*^
E37CA-L33CB*			E42CA-R44CA*^
E37CB-L33CB*^			E42CB-R44CA*^
E37CB-L33CG*^			

FIGURE 1

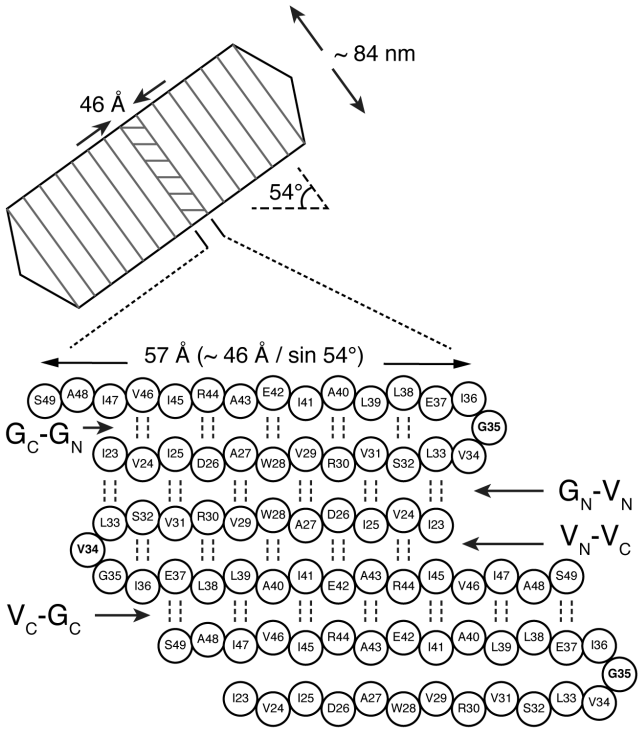
~ 84 nm
46 Å
54°
57 Å (~ 46 Å / sin 54°)
S49 A48 I47 V46 I45 R44 A43 E42 I41 A40 L39 L38 E37 I36
G35
I23 V24 I25 D26 A27 W28 V29 R30 V31 S32 L33 V34
G_C-G_N
G_N-V_N
V_N-V_C
L33 S32 V31 R30 V29 W28 A27 D26 I25 V24 I23
V34
G35 I36 E37 L38 L39 A40 I41 E42 A43 R44 I45 V46 I47 A48 S49
V_C-G_C
S49 A48 I47 V46 I45 R44 A43 E42 I41 A40 L39 L38 E37 I36
G35
I23 V24 I25 D26 A27 W28 V29 R30 V31 S32 L33 V34

FIGURE 2

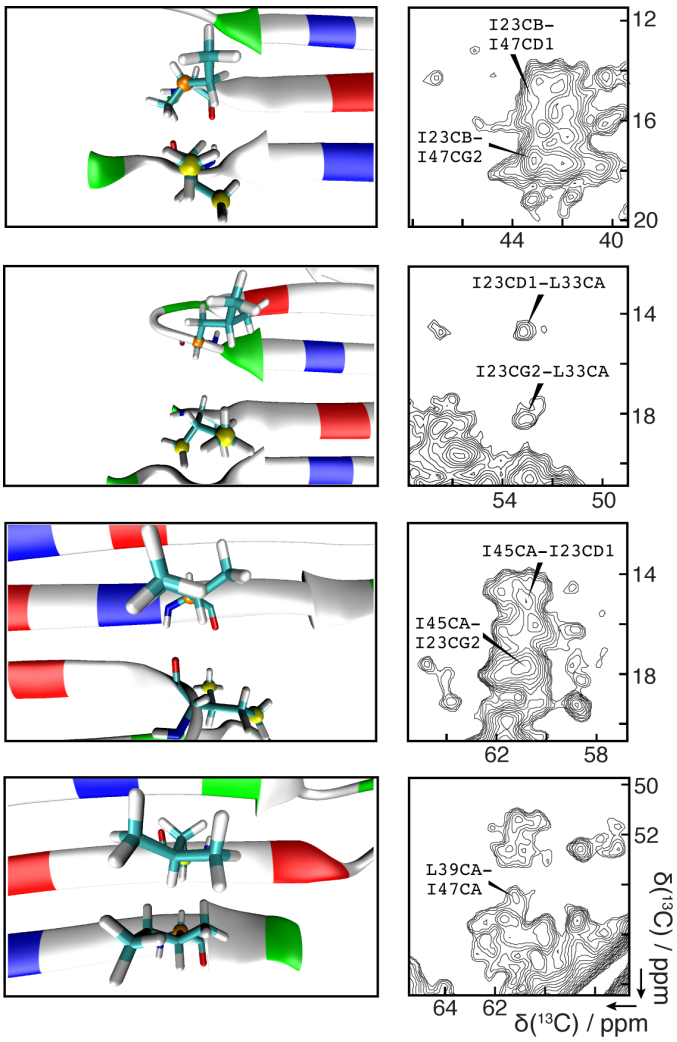
I23CB–
I47CD1
I23CB–
I47CG2
12
16
20
44
40
I23CD1–L33CA
I23CG2–L33CA
14
18
54
50
I45CA–I23CD1
I45CA–
I23CG2
14
18
62
58
L39CA–
I47CA
50
52
64
62
δ(13C) / ppm
δ(13C) / ppm

FIGURE 3

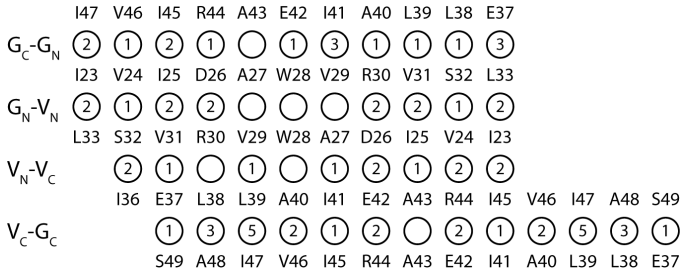
I47 V46 I45 R44 A43 E42 I41 A40 L39 L38 E37
G_C-G_N 2 1 2 1 0 1 3 1 1 1 3
I23 V24 I25 D26 A27 W28 V29 R30 V31 S32 L33
G_N-V_N 2 1 2 2 0 0 0 2 2 1 2
L33 S32 V31 R30 V29 W28 A27 D26 I25 V24 I23
V_N-V_C 2 1 0 1 0 1 2 1 2 2
I36 E37 L38 L39 A40 I41 E42 A43 R44 I45 V46 I47 A48 S49
V_C-G_C 1 3 5 2 1 2 0 2 1 2 5 3 1
S49 A48 I47 V46 I45 R44 A43 E42 I41 A40 L39 L38 E37

FIGURE 4